First-principles calculations of the initial incorporation of carbon into flat and stepped Pd surfaces

L. Nykänen,[1] J. Andersin,[1] and K. Honkala[1,2]
[1]*Department of Chemistry, Nanoscience Center, University of Jyväskylä, P.O. Box 35, FIN-40014 Jyväskylä, Finland*
[2]*Department of Physics, Nanoscience Center, University of Jyväskylä, P.O. Box 35, FIN-40014 Jyväskylä, Finland*
(Received 11 September 2009; revised manuscript received 1 December 2009; published 17 February 2010)

We employ density-functional-theory calculations to examine carbon adsorption and diffusion in Pd bulk, and on Pd(111) and Pd(211) surfaces. Different possible subsurface and on-surface structures are explored and the most stable structures are analyzed. We calculate various diffusion paths: lateral diffusion on a surface, migration to a subsurface region, and within the first interlayer. Our calculations show in accordance with the earlier theoretical results that on Pd(111) carbon prefers to adsorb on octahedral interstitial sites. On Pd(211) the fourfold hollow site under the step is energetically the most favorable one and the second best sites are the octahedral sites. The calculations indicate that migration into the first interlayer is more favorable than diffusion on the Pd(111) surface and migration into the second interlayer is already highly activated with barrier height close to those obtained in bulk. Nearly nonactivated diffusion paths into the first interlayer are found at the step edge of bare Pd(211) but carbon is found to diffuse easily from the first interlayer to the fourfold hollow site on Pd(211) thus leading to the decoration of step edges with carbon. Preadsorbed carbon increases the surface-subsurface diffusion barrier but it remains smaller than the corresponding value on bare Pd(111). At higher carbon concentration the mixed surface-subsurface structures are the most stable ones and carbon atoms tend to sit as far away from each other as possible.

DOI: 10.1103/PhysRevB.81.075417 PACS number(s): 34.50.Lf, 31.15.ae, 68.43.Jk, 68.43.Fg

I. INTRODUCTION

Increasing amount of evidence indicates that the near-surface modifications of a Pd-based catalyst with various carbonaceous deposits play a central role in several catalytic reactions.[1–4] The carbon residues originate from various possible side reactions. The modifications can lead to the deactivation and poisoning of the catalyst and substantial financial loss[5] but they have also been found to increase the catalytic performance.[1,6] The recent results of Teschner *et al.*[1] show that the formation of a PdC phase during alkyne hydrogenation is a general process and does not depend on the alkyne used. The results indicate that subsurface species determine the surface chemistry: unselective hydrogenation takes place on hydrogen-saturated β-hydride, whereas selective hydrogenation requires subsurface C to block subsurface H from participating to hydrogenation reaction and to modify the chemical properties of the catalyst. The density-functional-theory (DFT) calculations revealed that on a Pd with the selvedge PdC phase, the accumulation of H into the subsurface region is thermodynamically disfavored and the adsorption on the surface is weakened.[7] In ethene oxidation on Pd(111) the promotional effect of subsurface C is indirect. At high enough temperature the dissolved carbon diffuses back to the surface reducing oxygen adsorption that is essential to high activity.[8] In selective ethyne hydrogenation to ethene from ethyne/ethene mixture some of ethyne molecules decompose and decomposition products, carbon atoms, migrate into a Pd lattice.[2,3] The formation of PdC phase is also seen when Pd(111) interacts with C_2H_2, CO, and C_2H_4 molecules at elevated temperatures.[9] Also on Pd(110) various organic molecules have been found to lead to C deposition at high temperatures and UHV conditions.[10] Rose *et al.*[11] applied scanning tunnel microscope measurements to study the properties of the impurity species on the subsurface region of Pd(111). One of the species was most likely identified to be carbon and the lateral diffusion barrier of subsurface species was determined to be 0.72 eV. Experimentally derived barrier for a surface to subsurface diffusion is 1.1 eV at high carbon coverage.[12]

The early x-ray diffraction studies revealed the formation of Pd-C phase when Pd is heated in the atmosphere of ethylene.[9] The carbon content was reported to be ~13 at. % with carbon atoms residing in octahedral sites. In recent experiments on alkyne hydrogenation over Pd the subsurface carbon content is estimated to be around 40%.[13] The DFT calculations of Gracia *et al.*[14] on Pd(111) confirm the octahedral site as the best subsurface site with the adsorption energy of −7.15 eV. The calculations give a barrier of 0.74 eV for C diffusion from an octahedral site to a tetrahedral site in a very good agreement with the measured value. The calculated barriers for surface-subsurface diffusion and from the first interlayer spacing to the second one are 0.31 and 1.80 eV, respectively. The high diffusion barrier from the first to the second interlayer is suggested to follow from the fact that no in-plane relaxations are possible. Combining DFT calculations with cluster models (with the size of 79 or 116 Pd atoms) Yudanov *et al.*[15] found that C adsorption on a subsurface octahedral site is slightly more exothermic compared to the on-surface adsorption. The diffusion barrier for migration to subsurface was found to be 0.81 eV. Recently, DFT calculations were done for a carbon adsorption on a Pd_{140} cluster:[16] the subsurface adsorption is exothermic by 0.5 eV compared to surface adsorption and the adsorption energy of a carbon atom is found to depend on the distance from the cluster edge. The best adsorption energies for subsurface carbon are −7.60 and −7.35 eV for octahedral and tetrahedral sites, respectively. The results indicate that at the

cluster edge the stability of tetrahedral site is more enhanced than that of the octahedral site and that a surface-subsurface diffusion barrier is nearly zero.

In our earlier work we have shown that C_2H_4 decomposition takes place more efficiently and decomposition products bind stronger onto the stepped than onto the flat Pd surface.[17] This raises the question of the role of the steps in the adsorption and the diffusion of carbon on the surface and selvedge of Pd. Here the systematic study of carbon adsorption and initial corporation on flat and stepped Pd is presented. As the diffusion to a subsurface region is found to take place easily several structures with different on-surface-subsurface site combinations are addressed. We analyze the studied structures and discuss why some geometries are more stable than the others.

The paper is organized as follows. We start with analyzing and comparing the adsorption properties of atomic carbon on Pd(111) and Pd(211) surfaces. This is followed by the discussion on carbon diffusion both parallel and perpendicular to the surface at low coverage and at the presence of preadsorbed carbon. After that higher carbon concentration structures including both surface and subsurface species are presented and discussed. Finally we analyze and discuss the electronic structure of the selected systems.

II. COMPUTATIONAL METHODS

DFT calculations were carried out with the DACAPO code,[18] where Kohn-Sham equations are solved self-consistently using the revised Perdew-Burke-Ernzerhof (RPBE) (Ref. 19) generalized gradient correction to describe exchange and correlation effects. The plane-wave basis was restricted by a kinetic-energy cutoff of 25 Ry and the core electrons of the atoms were treated with Vanderbilt ultrasoft pseudopotentials.[20] For both the 111 and the 211 surfaces three models were used: a (3×2) supercell and a slab thickness of four or five layers (in the 111 lattice direction) and a (3×3) supercell with four layers. The periodic images were separated by 10 Å of vacuum to minimize the interactions between the successive metal slabs. The Brillouin zone was sampled at 16 Monkhorst-Pack k points in the case of (3×2) supercells and four Monkhorst-Pack k points for the (3×3) supercells. The two lowest metal layers were fixed to their ideal bulk positions (a=3.985 Å) while all the other atoms were relaxed until the residual force was below 0.05 eV/Å. To check the convergence we calculated several adsorption systems with cutoff energy of 400 eV and residual force 0.01 eV/A and found out that the adsorption energies change less than 0.02 eV. The bulk calculations were done with a supercell of 32 atoms and 64 Monkhorst-Pack k points. One Pd atom was fixed and the rest were relaxed. Transition states for the diffusion paths and reactions were determined by applying nudged elastic band method[21] and adaptive nudged elastic band method.[22] Note that at the transition state two or more Pd atomic shells are relaxed around the carbon atom. For the found transition states when harmonic frequencies were calculated only a single imaginary frequency was obtained in each case and the visualization of the frequency confirmed it to be along the reaction coordinate.

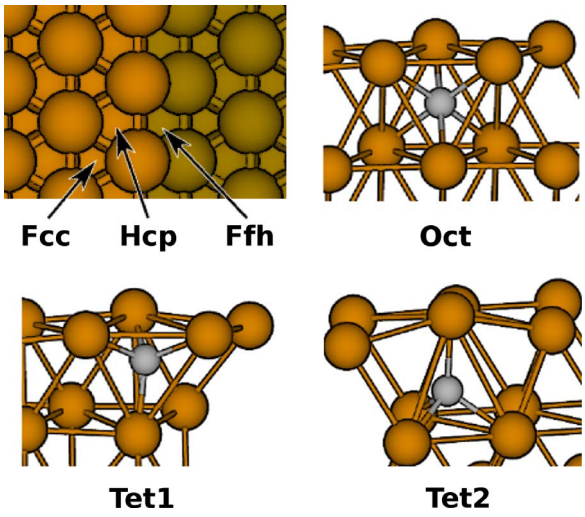

FIG. 1. (Color online) The relevant on-surface adsorption sites of fcc(211) slab (fcc, hcp, and Ffh) and subsurface sites in fcc lattice (Oct, Tet1, and Tet2). Surface atoms of different terraces are of different color. fcc and hcp sites are identical to the ones on Pd(111). In subsurface structures the carbon is presented in gray and the palladium atoms in ochre. Oct is an abbreviation for octahedral and Tet is for tetrahedral.

Averaged adsorption energies for C are calculated relative to C atom in gas phase infinitely far away from the surface. The averaged adsorption energy of C in a supercell containing N C atoms is calculated according to

$$E_{ads,\mathrm{C}} = \frac{E_{tot} - (E_{slab} + NE_{\mathrm{C}(g)})}{N},$$

where E_{tot} is the total energy of the adsorbate, the slab, E_{slab} refers to the energy of the clean slab, and $E_{\mathrm{C}(g)}$ is the energy of gas-phase C atom. The solution enthalpy is calculated similarly with

$$E_{ads,\mathrm{C}} = \frac{E_{tot} - (E_{bulk} + NE_{\mathrm{C}(g)})}{N},$$

where E_{bulk} is the energy of bulk Pd. For an exothermic (endothermic) reaction adsorption energy is negative (positive).

The amount of subsurface C is presented in atomic percents which we defined with equation

$$N_{\mathrm{C,at.\ \%}} = \frac{N_{\mathrm{C}}}{N_{\mathrm{Pd},sur} + N_{\mathrm{C}}} 100 \ \text{at. \%},$$

where N_{C} is the number of C atoms and $N_{\mathrm{Pd},sur}$ is the number of Pd surface atoms.

The relevant on-surface and subsurface adsorption sites are presented in Fig. 1. At the fcc and hcp sites the C atom is bonded to three Pd atoms whereas on the fourfold hollow (Ffh) site the C atom can bind to the four surface atoms or, when in plane with the four surface atoms, to five atoms including an atom deeper within the lattice. For subsurface C there are two possible sites available: (i) the octahedral site, denoted henceforth "Oct," which has six neighbor Pd atoms,

three below and three above, see Fig. 1, and (ii) the tetrahedral site, which has four neighbors. As can be seen from Fig. 1 there are two types of tetrahedral site: one with three Pd atoms above and one below (denoted "Tet1") and the other one has one Pd atom above and three below (denoted "Tet2").

III. RESULTS

In the following paragraphs we first discuss carbon solution and diffusion in bulk Pd. This is followed by the results of carbon adsorption and diffusion on and below Pd (111) and (211) surfaces at low coverage (θ=1/6 ML). Various high coverage (θ=1/3–2/3 ML) models including both surface and subsurface C are presented and discussed subsequently.

A. Carbon in bulk Pd

We start by discussing carbon diffusion in bulk Pd. The calculations are done with 3 at. % carbon concentration which corresponds to 32 Pd atoms per one carbon atom. The best adsorption site is the Oct site with the solution enthalpy of −6.42 eV with respect to gas-phase carbon atom and the Tet site is 0.92 eV less favorable. The diffusion barrier from one Oct site to the next one is 1.40 eV, which compares very well with measured value 1.32 eV (Ref. 23) and the calculated value 1.48 eV.[24]

The diffusion path goes through a Tet site, and at the transition state the C atom lies in the center of a triangle shared by the Oct and Tet sites and the Pd-C distance is 1.88 Å. The Pd atoms forming the triangle are displaced by 0.25 Å from their bulk positions radially away from the C atom. The comparison of the barriers shows that in bulk Pd the barrier is 0.4 eV smaller than in bulk Ni (4 at. % of C) (Ref. 25) and 0.4 eV higher than in bulk Fe (3 at. % of C).[26]

B. On-surface and subsurface carbon

On a Pd(111) surface C prefers to sit on a hcp site with the adsorption energy of −6.13 eV at 0.17 ML coverage. The average Pd-C distance is 1.92 Å and the average relaxation of the topmost Pd layer is 0.04 Å outward. At the best adsorption site, Ffh, on Pd(211) the Pd-C distance is 2.02 Å. Stolbov *et al.*[27] also found the Ffh site to be the most stable on Pd(211) with the adsorption energy of −9.1 eV using PW91 functional. Our adsorption energy is −7.04 eV being substantially smaller than that of Stolbov and co-workers. Presumably, the difference rises from the computational setup for a carbon atom (spin polarized/spin unpolarized) and the different generalized gradient approximation (GGA) functional. The Ffh site binds carbon 0.9 eV more strongly than the hcp site on Pd(111), a slightly larger difference, 1.0 eV, is found between Ni(111) and Ni(211) surfaces.[25] Adsorption energies of C on different transition-metal surfaces have been listed in Table I. It should be noted that most results were calculated with PW91 functional, which gives approximately 0.5 eV stronger binding than the RPBE functional.[19] The results indicate that Ni, Pd, and Pt are very similar whereas within groups 9 and 11 there is considerable variation. The adsorption energies are close to the cohesive energy of diamond which we calculated to be 7.27 eV [experimentally measured value is 7.37 eV (Ref. 28)].

TABLE I. Averaged adsorption energies of carbon on the hcp site of fcc(111) transition-metal surfaces from DFT calculations.

Metal	E_{ads} (eV)	Coverage (ML)	Functional
Co (Ref. 35)	−9.36	0.25	PW91
Rh (Ref. 36)	−7.18	0.10	PW91
Ir (Ref. 37)	−6.29	0.25	RPBE
Ni (Ref. 38)	−6.00	0.25	RPBE
Pd (Ref. 14)	−6.43	0.08	PW91
Pd (Ref. 39)	−6.61	0.25	PW91
Pd (Ref. 40)	−6.65	0.25	PW91
Pt (Ref. 41)	−6.18	0.25	RPBE
Pt (Ref. 41)	−6.75	0.25	PW91
Cu (Ref. 40)	−4.83	0.25	PW91
Cu (Ref. 42)	−4.51	0.25	PBE
Ag (Ref. 39)	−3.55	0.25	PW91

Energetics and various subsurface adsorption sites for carbon in Pd(111) and Pd(211) surfaces are summarized in Fig. 2. In the first interstitial region of Pd(111) a carbon atom prefers an Oct site with the adsorption energy of −6.86 eV that is 0.73 eV more favorable than the best on-surface site, hcp, and 0.44 eV more favorable than the Oct site in bulk Pd. Tet1 and Tet2 sites have adsorption energies −6.30 and −6.21 eV, respectively, which are around 0.6 eV less than found for the Oct site but more than 0.1 eV better than for the on-surface sites. Gracia *et al.*[14] reported adsorption energies −7.15, −6.74, and −6.63 eV for Oct, Tet1, and Tet2 sites, respectively. Again, our adsorption energies are larger than those given in literature but once again the reason is the different computational setup: we use a different unit cell and GGA functional compared to Ref. 14. In the second interlayer the binding to an Oct site is 0.2 eV weaker compared to the first interlayer. The corresponding value from Ref. 14 is 0.27 eV. The energy difference for the first and second interlayer Tet sites is ~0.4 eV. Note that adsorption energy on the Oct site in the second interlayer is ~0.5 eV better than that for the hcp site.

The average Pd-C distances are 2.06 (2.05), 1.92 (1.91), and 1.94(1.92) Å for Oct, Tet1, and Tet2 sites, respectively, in the first (second) interlayer and 1.92 Å for hcp site. The presence of C increases the distance between the surface Pd layer and the first subsurface Pd layer. The increase of 0.07, 0.15, and 0.12 Å compared to bare Pd(111) for Oct, Tet1, and Tet2 sites, respectively, is seen. In the case of Oct (Tet1) site the three surface atoms coordinated to C relax 0.16(0.33) Å outward whereas the Pd atom located right above the Tet2 site moves up by 0.63 Å.

On Pd(211) the best adsorption site for C is the Ffh site with the adsorption energy of −7.04 eV. On Pd(211) the binding energy of C varies from one Oct (or Tet) site to another depending on the location of the site from the step edge. Different subsurface sites together with C adsorption

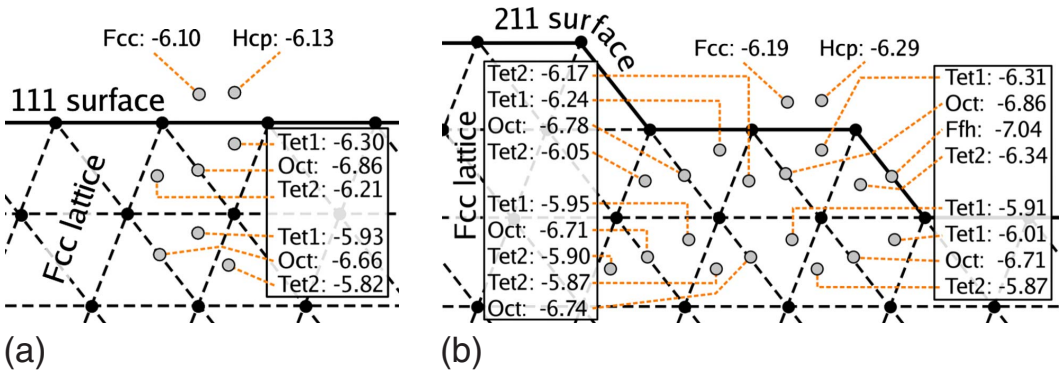

FIG. 2. (Color online) Side views of Pd(111) and Pd(211) slabs. Surface and subsurface sites are depicted with gray dots and corresponding adsorption energies are given for C in electron volt. These pictures are projections of the Pd lattices and adsorption sites to a plane perpendicular to the surface (and the steps). The actual lattice points and adsorption sites do not reside in a plane.

energies are given in Fig. 2. The second best site is the first Oct site behind the step with adsorption energy −6.86 eV and tetrahedral sites next to the step have adsorption energies −6.31 and −6.34 eV. Further away from the step the binding becomes weaker. In the second interlayer two Oct sites have binding energies −6.71 and −6.74 eV. This is still more favorable than adsorption on the hcp or fcc sites. The adsorption energies of tetrahedral sites vary slightly from −5.87 to −6.01 eV. Two carbon atoms at the step edge give average adsorption energy of −6.41 eV indicating a strong repulsion between carbons. At this step edge coverage adsorption is more exothermic than at lower coverage on the terrace but less exothermic than in the first and second interlayers.

To analyze the differences between on-surface and subsurface adsorption of C we plot atom projected density of states (DOS) in two cases: C on the hcp site on the Pd(111) surface and C in the Oct site below the surface (Fig. 3). In the figure the states are projected to the s and p orbitals of C and to the d orbitals of two topmost Pd layers. In general, the adsorption of C decreases the density of states at the Fermi level and the decrease is slightly larger in the case of subsurface adsorption. The interaction between carbon and palladium is similar both for on-surface and subsurface cases and takes place mainly via hybridization of the C $2p$ and Pd $4d$ states. In the case of subsurface C the bonding state is ≈ 2 eV below the bottom edge of the Pd d band, whereas the bonding orbital of the on-surface carbon is right below the bottom of the d band. The DOS analysis indicates that the interaction is polar covalent and between a subsurface C and Pd it is stronger than between on-surface C and Pd. The antibonding orbital is empty in both cases. This nicely agrees with our adsorption energies that give 0.7 eV stronger adsorption to the subsurface Oct site than to the on-surface hcp site.

Charge-density difference plots, see Fig. 4, for carbon on Oct, hcp, and Ffh sites provide an additional insight into bonding interactions between C and Pd atoms. The plots clearly indicate that the coordination of a carbon atom varies in these adsorption sites: in the subsurface Oct site carbon is symmetrically coordinated to six nearest Pd atoms. In the Ffh site the coordination number is 5 and on the hcp site it is 3. The changes in other Pd atoms than shown are negligible. All the plots show the charge accumulation between the C atom and Pd atoms supporting the covalent bonding. Each Pd atom coordinated to the C atom experience charge redistribution: depletion from the d_{z^2} orbital and accumulation to d_{xy}, d_{xz}, and d_{yz} orbitals. The charging of C atoms is modest: The Bader charges of the C atoms range from −0.34 to $-0.40e$ on the surface and from −0.64 to $-0.68e$ below surface. The negative charging of the C atoms is consistent with them being more electronegative than the Pd atoms. Also the near doubling of the charge below the surface is intuitive since the coordination is also doubled.

The calculations show that even at low coverage carbon adsorption in the bulk is more stable than on the Pd(111) surface indicating a clear thermodynamic driving force for migration of carbon into bulk Pd. The ranking of carbon stabilities goes from step sites to surface sites via subsurface and bulk sites and this might be important for the formation of PdC phase. As in the case of Ni(111) (Ref. 25) increased

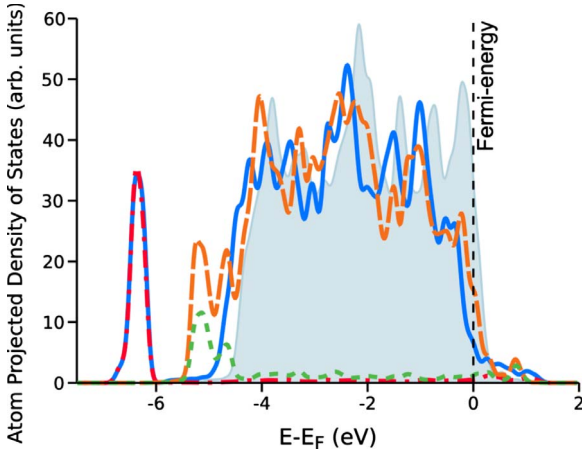

FIG. 3. (Color online) The atom projected density-of-states plots of a clean Pd(111) surface, a Pd surface with 25 at. % C adsorbed to on-surface sites and a Pd surface with 25 at. % C in subsurface layer. For the Pd surfaces the d bands of the two topmost atomic layers are plotted and for the C atoms the s and p bands. The dashed orange and green lines are the DOS of Pd and C, respectively, of the model with on-surface C. The blue solid line and the red dot and dash line are the DOS of Pd and C, respectively, of the model with subsurface C. The light blue area is the DOS of the clean Pd surface.

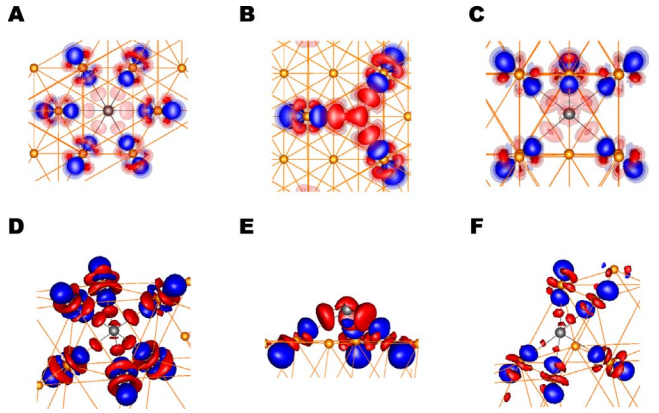

FIG. 4. (Color online) Charge-density difference figures of C adsorbed to Oct, hcp, and Ffh sites when viewed from the top (A to C, respectively) and from the side (D to E, respectively). The red (blue) color indicates the increase (decrease) in the electron density. In the top views the contours $\pm(0.01, 0.015, 0.02)ea_0^{-3}$ of the electron density are presented. In the side views the contours ± 0.01, ± 0.02, and $\pm 0.015ea_0^{-3}$ are presented for D, E, and F, respectively.

stability of carbon in the subsurface site compared to the hcp site on Pd(111) owes to higher coordination to Pd and an outward relaxation of the topmost Pd(111) layer. The behavior of C is somewhat unique since, for example, oxygen, sulfur, and hydrogen prefer adsorption to on-surface sites.[29–31] For O and S it has been shown that with coverage $\theta \geq 0.75$ ML it becomes more favorable for part of the atoms to reside at subsurface sites than to occupy on-surface sites only.

C. Diffusion

In the previous section, it was shown that adsorption to subsurface sites is clearly more favorable with respect to on-surface adsorption even at low carbon coverage. So the very first carbon could migrate into the lattice. Next, we focus on the diffusion of carbon atoms on a surface, from surface to interlayer sites, and between interlayer sites at 0.17 ML total coverage (corresponds 14 at. %). In few examples also higher carbon concentrations are shortly addressed. The Pd(211) models the step edge on a Pd nanoparticle and they might affect the diffusion properties partly because the steps bind carbon residues strongly. The schematic drawings of the studied diffusion paths are presented in Figs. 5 and 6 for the 111 and 211 surfaces, respectively. The figures are accompanied with tables (Tables II and III) where the type of the initial site and the final site, the diffusion barrier, and the reaction energy calculated between the initial and final states, ΔE, are given.

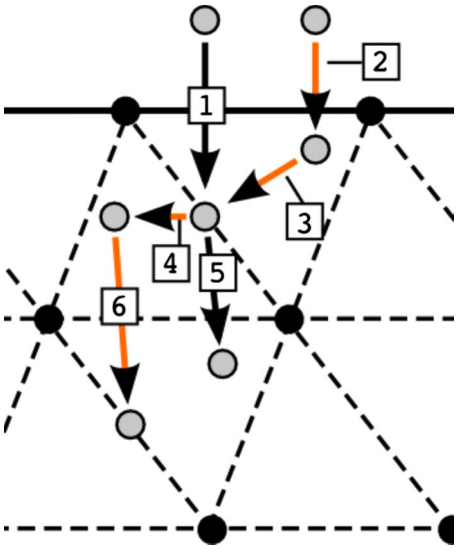

FIG. 5. (Color online) A schematic representation of the studied diffusion path ways from the (111) surface to the first and second interlayers.

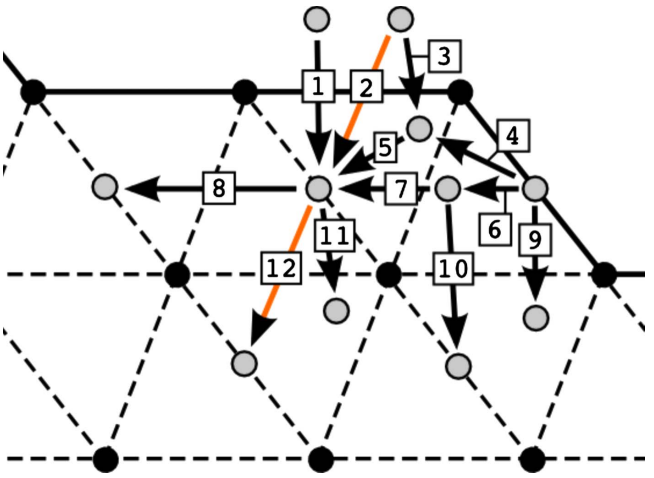

FIG. 6. (Color online) Schematic representation of the studied diffusion paths from on-surface sites to the first and second interlayers.

1. 111 surface

We start with the elementary diffusion steps and discuss the overall diffusion pathway at the end of the section. The surface diffusion barrier from the most stable adsorption site, hcp, to the second best site, fcc, is 0.77 eV and the process is almost thermoneutral. The value is in good agreement with 0.68 eV barrier reported in Ref. 24. In the transition state the C atom lies in the bridge site, i.e., coordinated to two Pd atoms, with the Pd-C distance 1.87 Å, which is 0.05 Å

TABLE II. Energetics of various diffusion paths depicted in Fig. 5 on Pd(111).

No.	Path	Barrier	ΔE
1	fcc → Oct	0.55	−0.76
2	hcp → Tet1	0.50	−0.16
3	Tet1 → Oct	0.26	−0.56
4	Oct → Tet2	0.81	0.63
5	Oct → Tet1	1.83	0.91
6	Tet2 → Oct	1.25	−0.45

TABLE III. Diffusion barriers on Pd(2111) for reaction paths given in Fig. 6.

No.	Path	Barrier	ΔE
1	fcc→Oct	0.10	−0.57
2	hcp→Oct	0.11	−0.59
3	hcp→Tet1	0.22	−0.02
4	Ffh→Tet1	0.94	0.73
5	Tet1→Oct	0	−0.55
6	Ffh→Tet2	0.77	0.70
7	Tet2→Oct	0.43	−0.52
8	Oct→Oct	0.97	0.08
9	Ffh→Tet1	1.49	1.07
10	Tet2→Oct	0.88	−0.35
11	Oct→Tet1	1.56	0.94
12	Oct→Oct	1.43	0.12

shorter than the Pd-C distance at the hcp (fcc) site.

The diffusion to the first interlayer region can take place either from a fcc or from a hcp site. The barrier of 0.55 eV is obtained for the direct carbon migration from the fcc site to the Oct site, see pathway 1 in Fig. 5. At the transition state the C atom is in the center of a triangle, equidistant from the three Pd atoms it is coordinated to. The Pd atoms relax radially away from carbon so that the average Pd-C distance is 1.86 Å and the first interlayer expands 1.9% compared to the clean surface. The second possible diffusion path goes from a hcp to an Oct site via a Tet1 site, see pathways 2 and 3 in Fig. 5. The corresponding diffusion barriers are 0.50 and 0.26 eV, respectively. At the transition state for the path with the higher barrier the C atom is 0.17 Å above the plane spanned by its three neighboring Pd atoms, the average Pd-C distance is 1.85 Å, and the Pd atom below the hcp site is displaced toward the C atom by 0.17 Å compared to a clean-surface position. In Ref. 14 the following barriers are reported 0.55 eV from a fcc to an Oct site and 0.31 eV from a hcp to a Oct site via a Tet1 site at 0.08 ML coverage. The transition state geometries are similar to those described above. The fact that the fcc and hcp sites are isoenergetic and that the diffusion barriers differ only little increases the probability to find subsurface carbon since diffusion to the first interlayer is not limited to one possible channel.

When comparing on-surface diffusion and subsurface incorporation the results indicate that the latter process is more favorable. However, this differs from Ni(111), where the on-surface diffusion is more preferable according to DFT calculations.[25] These diffusion properties together with the larger thermodynamic driving force toward subsurface adsorption on Pd might be among the key factors that make Ni a better catalyst for the formation of the carbon nanostructures. We note that on Pd, minor increase in temperature enables the competition between on-surface diffusion and subsurface incorporation at low coverage. At higher carbon concentrations with carbon occupying both on-surface and subsurface sites the diffusion barriers might differ more leading to a totally different picture. We addressed the role of the preadsorbed carbon to the diffusion in the following case: one C atom resides at an Oct site and the second carbon migrates from the next-nearest fcc to the first interlayer. The presence of preadsorbed subsurface carbon increases the barrier height to 0.70 eV, which is close to the diffusion barrier on the bare Pd(111) surface. At the transition state the Pd atom (to which both C atoms are initially coordinated) is 1.14 Å higher than the rest of surface Pd atoms, the migrating C is coordinated to three Pd atoms (including the protruding one) and has the average Pd-C distance 1.90 Å.

The carbon can diffuse laterally in the first interlayer or access the second interlayer. In the first case the path goes from one Oct site to another via a Tet1 (Tet2) site. The barrier is 0.82 (0.81) eV and at the transition state the C atom is in plane of a triangle shared by the Tet1 (Tet2) and the Oct sites. Average Pd-C distance at the transition state is 1.95(1.94) Å and the first Pd layer expands 6.2 (5.2)% outward. In Ref. 14 the diffusion barriers of 0.74 eV (via Tet1) and 0.86 (via Tet2) are reported. In Ref. 24 the barrier of 0.94 eV is given but the diffusion path was not specified. The barriers reported here and those in Ref. 14 differ from the experimentally determined barrier by less than 0.1 eV.[11] According to experiments C migration to the Pd(111) lattice is not limited to the first interlayer as PdC phase is seen extending to deeper layers.[13] The diffusion from the first to the second interlayer can take place via two paths. One route goes from an Oct site in the first interlayer to an Oct site in the second interlayer via a Tet2 site (Fig. 5, paths 4 and 6) with barrier 1.88 eV. The second route is from an Oct site in the first interlayer to a Tet1 site in the second interlayer. In this case barrier is 1.83 eV. In Ref. 14 the corresponding barriers are 2.32 and 1.93 eV. The difference between the present and previously published results might arise from the difference in computational setups.

2. 211 surface

As steps are found to break a C-C bond in C_2H_4 more easily than terrace sites,[17] one can expect to have CH_x radicals and carbon atoms near step edges, and thus the carbon diffusion into a subsurface region near the step edge might be a relevant process. All the studied diffusion paths are summarized in Fig. 6 and their energetics in Table III. Calculations show that carbon enters quite easily to the Oct site from hcp and fcc sites at the step edge (see Fig. 1). The diffusion barriers are around 0.1 eV. The presence of preadsorbed C in the Ffh site increases the diffusion barrier to 0.29 eV from the fcc to the Oct site. A large decrease in barrier height compared to Pd(111) is due to the lower coordination of metal atoms and thus the higher flexibility of step edge atoms. The step edge atoms are slightly displaced over the lower terrace and thus give room for the C to enter the lattice. The results indicate that C diffuses into the subsurface region of Pd near the steps regardless of the temperature. As the Ffh site is the most stable site on Pd(211), one may ask how easily it is accessible from the Oct site. The diffusion toward the step edge can proceed either via a Tet1 or Tet2 site. The corresponding barriers are 0.76 and 0.95 eV, respectively, see the reverse of the reaction pathways 5+4 and 7+6 in Fig. 6. The Ffh site can also be reached directly from

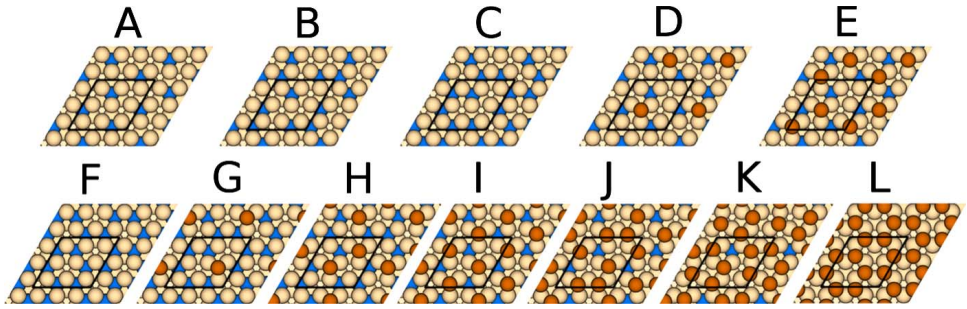

FIG. 7. (Color online) Top views of the most stable model systems with (1) all C atoms at subsurface positions for 25, 31, 36, and 40 at. % of C (A, B, C, and F, respectively), (2) both on-surface and subsurface carbon 25, 31, 36, and 40 at. % of C (A, D, E, and I, respectively), and (3) different distributions of C between on-surface and subsurface layers at 40 at. % of C (F–L). The light yellow spheres are Pd atoms, the blue ones are subsurface C, and the orange ones are on-surface C. The black rhombus depicts the supercell.

the hcp site via a Tet1 site, pathway 3 and reverse pathway 4 in Fig. 6. In this case the barrier is 0.22 eV.

To study diffusion from the first to the second interlayer we chose two starting points—the Oct site next to the step and the Ffh site. From both sites there are two pathways to the second interlayer (pathways 6+10, 9, 11, and 12 in Fig. 6) and in all cases the barrier is close to 1.5 eV, which is ~0.4 eV lower than found on Pd(111). The transition states resemble those of the 111 surface but the average Pd-C distances are ~0.05 Å longer than on a 111 surface, which reflects higher elasticity of lattice near the step leading to the lower migration barrier to the second interlayer.

D. Higher carbon concentrations

In order to gain insight to the stability of structures with higher concentration of carbon, we performed calculations on Pd(111) surface with various adsorption structures and the best ones are shown here. Based on experiments the concentration of carbon atoms in the selvedge is estimated to be around 40 at. % and carbon atoms are not restricted to the first interlayer.[13] However, no experimental results exist to provide the details of the structure and thus it is not known if any ordered phases are formed.

We use a (3×3) surface cell and systematically study many possible atomic configurations at 25, 31, 36, and 40 at. % of carbon, which correspond three to six carbon atoms in the (3×3) unit cell. We note that with a larger/smaller unit cell the formation of different surface-subsurface structures is possible. Although experimentally carbon atoms have been observed to penetrate into deeper interlayers, we focus on structures containing carbon atoms on surface and in the first interlayer.

We start with geometries involving 25 at. % of carbon. As in the case of 14 at. % of carbon in the (3×2) unit cell, carbon prefers to sit in an Oct site. With the increasing number of surface atoms and the decreasing number of subsurface atoms, the average adsorption energy changes linearly from −6.73 to −6.01 eV, see Fig. 8. The best adsorption structure is shown in Fig. 7(A). At 31 at. % (corresponds θ_{tot}=0.44 ML) the structure with all carbon atoms on subsurface sites is better than having all carbon atoms on the surface but the pure subsurface structure is not the energetically most favorable one. The best structure has three carbon atoms at subsurface sites and one on the surface, Fig. 7(D). The subsurface atoms sit on Oct sites and the on-surface atom on a fcc site.

For 36 at. % (corresponding θ_{tot}=0.56 ML) two structures are shown. In Fig. 7(C) all carbon atoms reside on subsurface sites and Fig. 7(E) gives the best adsorption structure for 36 at. % concentration with three atoms in subsurface and two atoms at on-surface sites. Note that the energy difference to pure subsurface adsorption and to the mixed adsorption with four subsurface carbons and one on-surface carbon is minor, only 0.05 and 0.03 eV, respectively. Somewhat larger energy difference, 0.18 eV, is found to the mixed structure of two subsurface and three on-surface carbons.

At highest studied carbon concentration six carbon atoms, corresponding 40 at. %, are distributed between surface and subsurface sites. Figures 7(F)–7(L) show a set of structures with 40 at. % of carbon and different distributions between on-surface and subsurface sites. The notable feature is that the best structure, Fig. 7(I), has both surface and subsurface carbons forming a $(\sqrt{3}\times\sqrt{3})R30$ structure. This mixture has three carbons at on-surface and subsurface sites. The binding energy of the structure in Fig. 7(I) exceeds slightly those cases where more carbon is in the subsurface region, see Figs. 7(F)–7(H). Structures in Figs. 7(H) and 7(J) are mirror images: in structure H (J) four (two) carbons are in the subsurface and two (four) in the surface region and atoms are distributed identically in both cases. The average adsorption energies differ by 0.33 eV structure H being energetically more favorable with larger number of subsurface carbon atoms. Structures G and K form also a pair with 5(1)/1(5) subsurface/surface mixture. However, the situation is slightly different since the structures are not mirror images. Structure K has one carbon on a hcp site and the rest surface atoms in fcc sites which improves the optimization of C-C distances. In structure G all subsurface carbons are in Oct sites since tetrahedral sites are energetically considerably less favorable.

The adsorption of carbon induces the expansion of the Pd lattice in the [111] direction and its extent depends on the C concentration and distribution between the subsurface and surface sites. Table IV summarizes the relative shifts in the first and second interlayer displacements compared to the clean Pd(111) surface. As expected, the expansion is most pronounced for the first interlayer with subsurface carbon reaching almost 13% at the highest concentration. The inter-

TABLE IV. The expansion of the first and second interlayers of Pd(111) containing C compared to the clean surface. The values are given for systems with only subsurface C, only on-surface C, and the energetically best structures.

Concentration of C (at. %)	Expansion in [111] direction (%)					
	Subsurface		On surface		Best	
	First	Second	First	Second	First	Second
25	6.4	2.5	1.6	0.5	6.4	2.5
31	9.0	3.2	3.2	0.7	7.6	2.7
36	11.7	3.7	3.6	0.7	8.6	2.7
40	12.9	4.0	3.4	0.5	9.3	2.7

layer expansion of the mixed structures decreases monotonically as the fraction of C at on-surface sites increases.

Figure 8 summarizes the best adsorption energies for each carbon concentration and distribution. Clearly with increasing coverage the adsorption becomes weaker and at all studied coverages subsurface adsorption is more favorable than on-surface adsorption. The two major decisive factors that determine adsorption energy are the position of a carbon atom: either on surface or subsurface and the C-C distance. With higher carbon concentrations than 25 at. % it becomes more favorable to have carbon atoms distributed between surface and subsurface sites. The investigation of the C-C distance for given structures in Fig. 8 reveals that the best adsorption energies are found for structures in which carbon atoms are distributed as evenly as possible. The energetic preference is partly determined by electronic repulsion but probably also the competition for d electrons of Pd atoms pushes carbon atoms apart. Among systems that share the highest C-C distance those configurations with $(\sqrt{3}\times\sqrt{3})R30$ subsurface structure and the rest of the carbon atoms at on-surface sites are energetically the best ones. At low concentrations hcp sites are slightly preferred to fcc sites. However, at higher concentrations the site shift takes place and fcc site becomes more favorable because carbon atoms residing in Oct sites destabilize all hcp sites in the vicinity: the carbon-carbon distance becomes too short and electrostatic repulsion pushes atoms away from hcp sites.

Finally we plotted the work functions of Pd(111) slabs with different C concentrations and different distributions of C between on-surface and subsurface sites (see Fig. 9) with aim to investigate the changes in surface reactivity compared to bare Pd(111). The subsurface C introduces minor, less than 0.26 eV, negative work-function change compared to the clean Pd surface. Only modest dependence on the carbon concentration is seen. With increasing surface coverage and decreasing subsurface content of carbon the work-function change shifts from negative to positive. When all carbon atoms are on the surface the work-function change is at most 0.68 eV for highest C coverage. The behavior of work function is similar to the one calculated for oxygen on and below Pd(111) (Ref. 29) surface but in our case the changes are

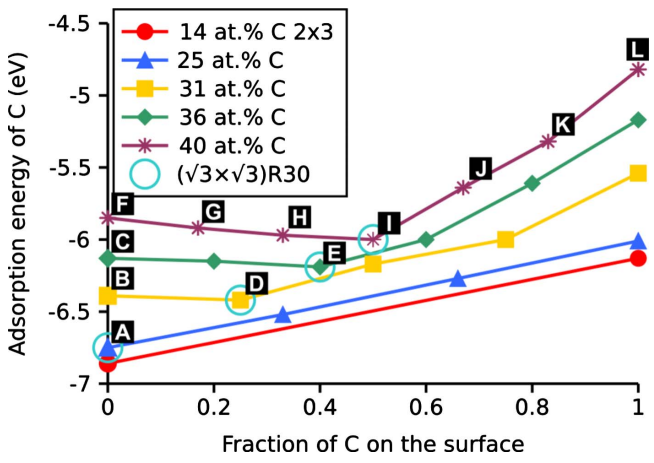

FIG. 8. (Color online) Averaged adsorption energies of C on 111 surfaces containing C both on and below surface. The energies are given as a function of C atoms on surface divided by the total number of C atoms $[N_{C,s}/(N_{C,s}+N_{C,ss})]$. Some points in the plot are accompanied with a letter and the structures of those systems are presented in Fig. 7. The circled points represent energy minimums of the different C concentrations.

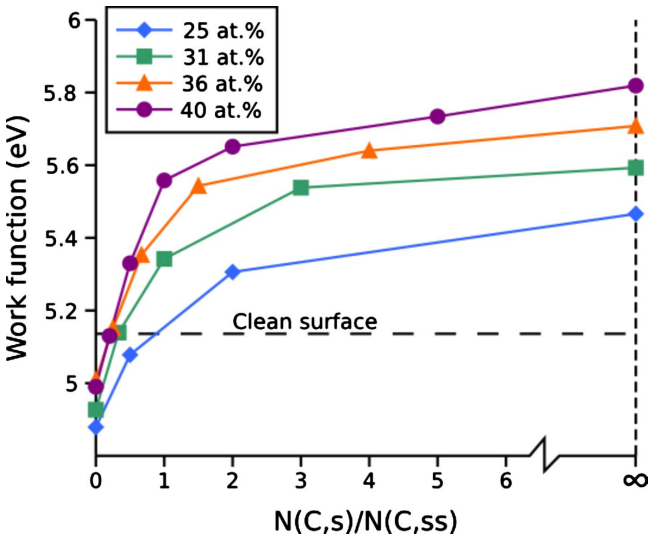

FIG. 9. (Color online) The work functions of Pd(111) surfaces containing different amounts of C are plotted against the distribution between subsurface and on-surface sites. On the x axis the zero value corresponds to all atoms being located at the subsurface layer and the infinity corresponds to all atoms being on the surface. Work function of the clean surface is presented with the dashed horizontal line.

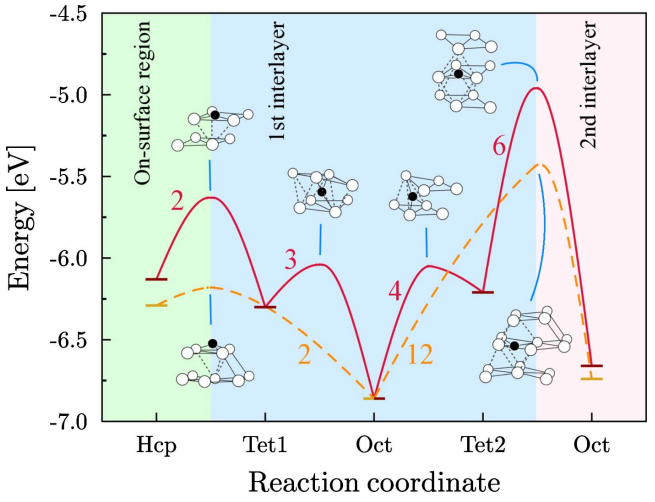

FIG. 10. (Color online) The energetics of diffusion from an hcp site to the second interlayer on 111 (red, solid line) and 211 surface (orange, dashed line) presented with potential-energy surfaces. Each diffusion step is accompanied with an illustration of the transition state structure and a number referring to the paths in Figs. 5 and 6. In the structures the black (white) spheres are carbon (palladium) atoms and only relevant atoms are shown.

much more minor presumably due to the lower electronegativity of carbon compared to oxygen. As the higher work function generally implies lower chemical reactivity, we may conclude that C atoms adsorbed on the metal leads to a more inert surface. The *d*-band center of the carbon containing Pd surface moves down compared to clean surface which further supports the assumption that the C adsorption leads to lower activity. The *d*-band center of the two uppermost Pd layers in a clean slab is −2.1 eV below the Fermi level. The corresponding value for the slab containing 40 at. % carbon in the most stable configuration is −3.5 eV. Comparison between the *d*-band centers of the unmixed structures indicates that the largest contribution to the drop in the *d*-band center comes from the carbons located on the surface.

IV. DISCUSSION AND SUMMARY

A one-dimensional potential-energy surface for pathways from on-surface sites to second interlayer involving the lowest overall barriers is presented in Fig. 10. The barriers are associated with the illustrations of the corresponding transition states. In agreement with previous DFT calculations[14] the overall picture emerging from our calculations is that at low coverage carbon adsorption in bulk is more exothermic than on-surface adsorption suggesting thermodynamic driving force for subsurface migration. In fact the Oct sites in the first interlayer are more stable than on-surface sites but less stable than Ffh sites at the step edge and this might affect the formation of a PdC phase. The C incorporation to the first interlayer has the lowest barrier, the steps being particularly effective in the process, whereas on both surfaces migration to the second interlayer is highly activated.

The low diffusion barrier to the first interlayer together with larger stability of Oct sites clearly indicate the occupation of near-surface region of Pd with carbon atoms. However, the low barrier contradicts the proposition of Gabasch *et al.*[12] who assume the migration barrier from the surface to the subsurface region be the rate-limiting step for the C incorporation to bulk Pd and thus the barrier is larger than for bulk-bulk diffusion. They note that from the experimental viewpoint the rate of carbon incorporation to the subsurface region must be the smallest one compared to any reaction step starting from molecular ethene. Our results indicate that the migration to the second interlayer is the rate-limiting step in C migration into deeper layers. The activation barrier is larger than that for bulk diffusion. It is also larger than any barrier in ethylene decomposition process, where highest barriers in processes (CH, CCH, and C_2 decomposition) forming atomic carbons are around 1.5 eV.[17,32] We note that in the measurements carbon coverage is high whereas our calculations are mainly done at low coverage. The case study shows that the presence of preadsorbed carbon increases the diffusion barrier to the first interlayer. However, based on present calculations it is not possible to say whether the diffusion from the surface to the first interlayer will have higher barrier than the diffusion from the first to the second interlayer at high carbon coverage. We also note that our barrier for the rate-limiting step (if compared to C in the first interlayer) is 0.7 eV higher than the barrier derived from experiments. Again including the coverage effects into calculations might change the barrier dramatically yet in this particular case the presence of carbons should decrease the calculated barrier.

In agreement with the recent cluster calculations[16] we find the diffusion into first interlayer nearly nonactivated over the Pd(211) at low coverage. The small diffusion barrier and the strong binding to Ffh sites at step edges suggest the decoration and blocking on step sites with carbon. Consequently, this will have an effect on all bond breaking reactions containing carbon, such as ethylene decomposition,[17] over the edges of Pd nanoparticles. Preadsorbed carbon on the Pd step increases the diffusion barrier to subsurface region but the barrier is still smaller than that calculated on a Pd terrace.

Since the population of the first interlayer with C is relatively easily activated we may assume that the process takes place immediately after carbon atoms become available. This incorporation may act as a first step in the formation of the PdC phase, whose exact geometric arrangement has remained unknown. The review over different C distributions at the Pd(111) reveals that there is a tradeoff between the C-C distance and the position of C atoms. Carbon atoms favor subsurface sites in the first interlayer but as the C concentration increases it becomes beneficial to accommodate also the surface sites. However, the evaluation of the structure and the formation of the realistic PdC phase structure probably requires the use of Monte Carlo simulations[33,34] and is beyond the scope of this paper.

To summarize we presented density-functional-theory study addressing carbon adsorption and diffusion in bulk Pd, on flat and stepped Pd surfaces and the incorporation of carbon to the Pd surface. The results show that at low coverage subsurface adsorption on an Oct site is more favorable than adsorption on Pd(111) or solution to bulk. At stepped Pd surface the best site is a Ffh site under the step, which is

better than any subsurface site. At higher carbon concentration various mixed structures were studied and the best structures are those with both subsurface and on-surface carbon and a long C-C distance. Large decrease in barrier height on the Pd step compared to the Pd terrace results from the lower coordination of step atoms which facilitates the relaxation of edge atoms. Thermodynamic driving force toward a Ffh site together with relatively low diffusion barriers from subsurface sites to the Ffh site ensure that at low coverage and high reaction temperature carbon atoms from surface and subsurface sites end up to Ffh sites under the Pd step. Diffusion barrier increases fast when incorporating deeper in to bulk: from the first to the second subsurface layer the barrier heights are equal or higher than those in bulk diffusion. Our calculations show that carbon migration into Pd is a complicated, coverage-dependent process, where the role of the low coordinated Pd atoms is important at the onset of carbon dissolution to Pd. Constructing a realistic PdC structure, including carbon migration to many subsurface layers is a challenging task and beyond present density-functional-theory calculations.

ACKNOWLEDGMENTS

This work was financially supported by the Väisälä Foundation through the Finnish Academy of Science and Letters and the Academy of Finland through projects 110653 and 118532. The computational resources were provided by the Nanoscience Center University of Jyväskylä and the Finnish IT Center for Science (CSC) Espoo.

[1] D. Teschner, J. Borsodi, A. Wootsch, Z. Revay, M. Hävecker, A. Knop-Gericke, S. D. Jackson, and R. Schlögl, Science **320**, 86 (2008).
[2] A. Borodziński and G. C. Bond, Catal. Rev.- Sci. Eng. **48**, 91 (2006).
[3] A. Borodziński and G. C. Bond, Catal. Rev.- Sci. Eng. **50**, 379 (2008).
[4] G. C. Bond, Appl. Catal., A **149**, 3 (1997).
[5] P. Albers, J. Pietsch, and S. F. Parker, J. Mol. Catal. A: Chem. **173**, 275 (2001).
[6] M. Wilde, K. Fukutani, W. Ludwig, B. Brandt, J. H. Fischer, S. Schauermann, and H. J. Freund, Angew. Chem., Int. Ed. **47**, 9289 (2008).
[7] D. Teschner, Z. Revay, J. Borsodi, M. Hävecker, A. Knop-Gericke, R. Schlögl, D. Milroy, S. D. Jackson, D. Torres, and P. Sautet, Angew. Chem., Int. Ed. **47**, 9274 (2008).
[8] H. Gabasch, A. Knop-Gericke, R. Schlögl, W. Unterberger, K. Hayek, and B. Klötzer, Catal. Lett. **119**, 191 (2007).
[9] S. B. Ziemecki, G. A. Jones, D. G. Swartzfager, and R. L. Harlow, J. Am. Chem. Soc. **107**, 4547 (1985).
[10] M. Bowker, C. Morgan, N. Perkins, R. Holroyd, E. Fourre, F. Grillo, and A. MacDowall, J. Phys. Chem. B **109**, 2377 (2005).
[11] M. K. Rose, A. Borg, T. Mitsui, D. F. Ogletree, and M. Salmeron, J. Chem. Phys. **115**, 10927 (2001).
[12] H. Gabasch, K. Hayek, B. Klötzer, A. Knop-Gericke, and R. Schlögl, J. Phys. Chem. B **110**, 4947 (2006).
[13] D. Teschner, E. Vass, M. Hävecker, S. Zafeiratos, P. Schnörch, H. Sauer, A. Knop-Gericke, R. Schlögl, M. Chamam, A. Wootsch, Arran S. Canning, Jonathan J. Gamman, S. David Jackson, James McGregor, and Lynn F. Gladden, J. Catal. **242**, 26 (2006).
[14] L. Gracia, M. Calatayud, J. Andrés, C. Minot, and M. Salmeron, Phys. Rev. B **71**, 033407 (2005).
[15] I. Y. Yudanov, K. M. Neyman, and N. Rösch, Phys. Chem. Chem. Phys. **6**, 116 (2004).
[16] F. Viñes, C. Loschen, F. Illas, and K. M. Neyman, J. Catal. **266**, 59 (2009).
[17] J. Andersin, N. Lopez, and K. Honkala, J. Phys. Chem. C **113**, 8278 (2009).
[18] https://wiki.fysik.dtu.dk/dacapo
[19] B. Hammer, L. B. Hansen, and J. K. Nørskov, Phys. Rev. B **59**, 7413 (1999).
[20] D. Vanderbilt, Phys. Rev. B **41**, 7892 (1990).
[21] H. Jónsson, G. Millis, and K. W. Jacobsen, in *Classical and Quantum Dynamics in Condensed Phase Simulations*, edited by B. J. Berne, G. Ciccotti, and D. F. Coker (World Scientific, Singapore, 1998).
[22] P. Maragakis, S. A. Andreev, Y. Brumer, D. R. Reichman, and E. Kaxiras, J. Chem. Phys. **117**, 4651 (2002).
[23] H. Yokoyama, H. Numakura, and M. Koiwa, Acta Mater. **46**, 2823 (1998).
[24] O. V. Yazyev and A. Pasquarello, Phys. Status Solidi B **245**, 2185 (2008).
[25] F. Abild-Pedersen, J. K. Nørskov, J. R. Rostrup-Nielsen, J. Sehested, and S. Helveg, Phys. Rev. B **73**, 115419 (2006).
[26] D. E. Jiang and E. A. Carter, Phys. Rev. B **67**, 214103 (2003).
[27] S. Stolbov, F. Mehmood, T. S. Rahman, M. Alatalo, I. Makkonen, and P. Salo, Phys. Rev. B **70**, 155410 (2004).
[28] L. Brewer, Lawrence Berkley Laboratory Report No. LB-3720, 1977 (unpublished).
[29] M. Todorova, K. Reuter, and M. Scheffler, Phys. Rev. B **71**, 195403 (2005).
[30] D. Alfonso, Surf. Sci. **600**, 4508 (2006).
[31] S. Hong and T. S. Rahman, Phys. Rev. B **75**, 155405 (2007).
[32] J. Andersin and K. Honkala, Surf. Sci. (to be published).
[33] K. Reuter and M. Scheffler, Phys. Rev. B **73**, 045433 (2006).
[34] J. Rogal, K. Reuter, and M. Scheffler, Phys. Rev. B **77**, 155410 (2008).
[35] J. C. W. Swart, I. M. Ciobîcă, R. A. van Santen, and E. van Steen, J. Phys. Chem. C **112**, 12899 (2008).
[36] A. Resta, J. Gustafson, R. Westerström, A. Mikkelsen, E. Lundgren, J. N. Andersen, M.-M. Yang, X.-F. Ma, X.-H. Bao, and W.-X. Li, Surf. Sci. **602**, 3057 (2008).
[37] W. P. Krekelberg, J. Greeley, and M. Mavrikakis, J. Phys. Chem. B **108**, 987 (2004).
[38] D. W. Blaylock, T. Ogura, W. H. Green, and G. J. O. Beran, J. Phys. Chem. C **113**, 4898 (2009).
[39] P. A. Sheth, M. Neurock, and C. M. Smith, J. Phys. Chem. B **109**, 12449 (2005).
[40] Z.-X. Chen, K. M. Neyman, K. H. Lim, and N. Rösch, Langmuir **20**, 8068 (2004).
[41] D. C. Ford, Ye Xu, and M. Mavrikakis, Surf. Sci. **587**, 159 (2005).
[42] N. M. Galea, D. Knapp, and T. Ziegler, J. Catal. **247**, 20 (2007).